Electronic structure and x-ray magnetic circular dichroism in Heusler-type $Fe_{2-x}V_{1+x}Al$: First-principles calculations

V. N. Antonov,[1] A. Ernst,[2,*] I. V. Maznichenko,[3,4] A. N. Yaresko,[5] and A. P. Shpak[1]
[1]*Institute of Metal Physics, 36 Vernadsky Street, 03142 Kiev, Ukraine*
[2]*Max-Planck Institut für Mikrostrukturphysik, Weinberg 2, D-06120 Halle, Germany*
[3]*Martin-Luther-Universität Halle-Wittenberg, Fachbereich Physik, D-06099 Halle, Germany*
[4]*Institute of Physics at Southern Federal University, 194 Stachky Avenue, Rostov-on-Don 344090, Russia*
[5]*Max Planck Institute for the Physics of Complex Systems, D-01187 Dresden, Germany*
(Received 11 July 2007; revised manuscript received 10 March 2008; published 28 April 2008)

Soft x-ray absorption spectra and their x-ray magnetic circular dichroism (XMCD) have been theoretically studied at the transition-metal $L_{2,3}$ thresholds of the Heusler-type $Fe_{2-x}V_{1+x}Al$. The electronic structure of $Fe_{2-x}V_{1+x}Al$ upon changing the content x was theoretically investigated from first principles by using the fully relativistic Dirac linear-muffin-tin-orbital band structure method and the scalar relativistic Korringa–Kohn–Rostoker method within the coherent potential approximation generalized to treat disorder in multicomponent complex alloys. Densities of valence states and spin and orbital magnetic moments are analyzed and discussed. The origin of the XMCD spectra in the $Fe_{2-x}V_{1+x}Al$ compound is examined. The calculated results are compared to the experimental data.

DOI: 10.1103/PhysRevB.77.134444 PACS number(s): 75.30.Mb, 71.28.+d

I. INTRODUCTION

The compounds Fe_2VZ (Z=Al,Ga) show marginal magnetic properties between the ferromagnetic and the nonparamagnetic or paramagnetic states.[1,2] The resistivity increases by a factor of 6 from 400 to 2 K (where ρ=3 mΩ cm), which is a characteristic of a nonmetal, but other properties indicate a metallic character. A sharp Fermi cutoff is observed in the photoemission spectrum and the specific heat coefficient $\gamma(T)=C/T$ more than doubles below 6 K (to 12 mJ/mol K^2). The nuclear magnetic resonance[3,4] and Hall-effect[5] measurements strongly supported that Fe_2VAl is characterized as a low carrier-density semimetal. Optical conductivity[6,7] and photoemission spectroscopy[8] measurements further confirmed the existence of a pseudogap of 0.1–0.2 eV in width. Nevertheless, the pseudogap scenario itself could not account for a steep rise in resistivity at low temperatures.[1]

The stoichiometric compound itself has no magnetic transition, while the alloy system $Fe_{2-x}V_{1+x}Al$ and the isoelectronic system $Fe_{2-x}V_{1+x}Ga$ are ferromagnetic,[9,10] with a Curie temperature that extrapolates to zero as $x\rightarrow 0^+$. The behaviors of ρ and C/T were suggested to be similar to those of heavy fermion metals, making these alloys as candidates for 3d based heavy fermion systems.[1,2] Another attractive feature of $Fe_{2\pm x}V_{1\mp x}Al$ and $Fe_{2\pm x}V_{1\mp x}Ga$ is the anomalous giant magnetoresistance (GMR) effect. Endo *et al.*[10] first found a massive negative magnetoresistance of Fe_2VGa reaching 48% for 20 T at 6.8 K. Recently, a similar GMR behavior was also observed in an Al-based alloy, $Fe_{2.1}V_{0.9}Al$, wherein the magnetoresistance reached approximately 40% for 13 T at 4.2 K.[11] For these alloys, the GMR effect occurs around a critical Fe concentration at $x\sim x_C$, in which the long-range ferromagnetic ordering arises.

Feng *et al.*[7] reported a variety of measurements on Fe_2VAl, including atomic emission spectroscopy, Fourier-transform infrared (FTIR) reflectance, x-ray diffraction, magnetization, and conductivity measurements. An analysis of the FTIR and dc resistivity suggests that the transport properties of Fe_2VAl are influenced by both localized and delocalized carriers, with the former primarily responsible for the negative temperature coefficient of the resistivity. Magnetization measurements reveal that near-stoichiometric samples have superparamagnetic clusters with at least two sizes of moments. This indicates that the antisite disorder in Fe_2VAl causes a significant modification of the semimetallic band structure that is theoretically proposed. With the antisite disorder considered, they were able to explain most of the physical properties of Fe_2VAl. None of their data supports a heavy-fermion behavior in Fe_2VAl.

Nishino *et al.*[12] investigated the magnetization, electrical resistivity, and specific heat for annealed samples of $Fe_{2-x}V_{1+x}Al$ with compositions $0.01\leq x\leq 0.08$. They found that the resistivity for a slightly V-rich sample of $Fe_{2-x}V_{1+x}Al$ with x=0.02 is reduced to only 300 mV cm at 4.2 K, which is almost an order of magnitude lower than that for a nominally more stoichiometric sample. It was suggested that the resistivity behavior of Fe_2VAl can be significantly affected by a small deviation in the chemical composition, which would result in the generation of magnetic antisite defects.

According to band structure calculations,[13–18] Fe_2VAl is a nonmagnetic semimetal with a pronounced pseudogap right at the Fermi level E_F. Guo *et al.*[13] and Singh and Mazin[14] reported local density functional results that indicated that Fe_2VAl is a low carrier density compensated semimetal. Γ-centered holes of the Fe t_{2g} antibonding character are compensated by zone-edge X-point holes of the V e_g character. Guo *et al.*[13] excluded electron-phonon coupling and expected spin fluctuations in Fe_2VAl to be the main reason for the enhanced effective mass, while the negative temperature coefficient of the resistivity is due to carrier localization. Singh and Mazin[14] argued that due to nonstoichiometry and antisite defects, magnetic moments may be responsible for a large

effective mass and the complex transport properties from low-density carriers interacting with localized magnetic moments. Weht and Pickett[15] proposed dynamic correlations between holes and electrons to be responsible for the resistivity. Bansil *et al.*[17] treated the substitution of Fe with V within the coherent-potential approximation. Recognizing the possibility of samples having stoichiometry problems and antisite defects, they concluded that Fe_2VAl may have the character of a heavy fermion material.

Recent theoretical studies of the $Fe_{2\pm x}V_{1\mp x}Z$ (Z=Al, Ga) compounds with a supercell approach[11,19] predicted that antisite defects or excess atoms in the Heusler lattice may induce a radical change in the electronic and magnetic properties. Indeed, Sum *et al.*[20] observed a remarkable decrease in the resistivity and magnetization at the nominal content $x=0.02$, indicating the formation of magnetic clusters. On the other hand, the MCD measurement for a scraped surface of Fe_2VAl reveals fairly large magnetic moments of $1.0\mu_B$ for Fe and $0.15\mu_B$ for V.[21]

The aim of the present electronic structure calculations is to extend the supercell calculations reported in Refs. 11 and 19 to a lower vanadium concentration range in the $Fe_{2-x}V_{1+x}Al$ compound for the composition $0 \le x \le 0.125$, which was not covered in previous calculations. Recently, in order to study the magnetic structure in $Fe_{2-x}V_{1+x}Al$ compound, soft x-ray absorption spectra and their x-ray magnetic circular dichroism were studied at the transition-metal $L_{2,3}$ thresholds.[22] The observed XMCD intensity changes as the bulk magnetization upon changing the content x in $Fe_{2-x}V_{1+x}Al$. Although the observed XMCD signals are small, they definitely indicate the antiferromagnetic coupling between the Fe and V magnetic moments. In the present study, we focus on the theoretical investigation of the x-ray magnetic circular dichroism in the $Fe_{2-x}V_{1+x}Al$ compounds.

This paper is organized as follows: The crystal structure of the $Fe_{2-x}V_{1+x}Al$ alloys and computational details are presented in Sec. II. Next, the electronic structure of the $Fe_{2-x}V_{1+x}Al$, which is obtained by using the fully relativistic Dirac linear-muffin-tin-orbital (LMTO) band structure method and scalar relativistic Korringa–Kohn–Rostoker method within the coherent potential approximation (CPA-KKR) approach, is discussed in Sec. III A. Section III B is concerned with x-ray magnetic circular dichroism (XMCD) spectra of these alloys that are estimated with the fully relativistic Dirac LMTO method. The calculated results are compared to the available experimental data. Finally, the results are summarized in Sec. IV.

II. CRYSTAL STRUCTURE AND COMPUTATIONAL DETAILS

The Heusler-type X_2YZ compounds crystallize in the cubic $L2_1$ structure with the space group $Fm\bar{3}m$ (No. 225). It is formed by four interpenetrating fcc sublattices. The X ions occupy the $8c$ Wyckoff positions ($x=1/4$, $y=1/4$, $z=1/4$). The Y ions occupy the $4a$ positions ($x=0$, $y=0$, $z=0$), and the Z ions are placed at the $4b$ sites ($x=1/2$, $y=1/2$, $z=1/2$). All atoms have eight nearest neighbors at the same distance. The Y and Z atoms have eight X atoms as the nearest neighbors, while for X there are four Y and four Z atoms.

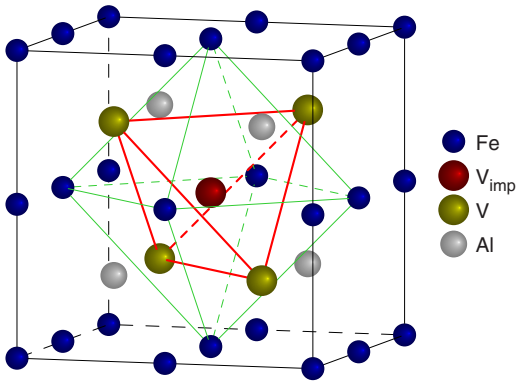

FIG. 1. (Color online) Schematic of the $Fe_{2-x}V_{1+x}Al$ structure for $x=0.25$. The V and Fe nearest neighbors of the V impurity are connected by the thick and thin lines, respectively.

The details of the computational method are described in our previous papers,[23,24] and here, we only mention several aspects. The calculations of the electronic structure of the Fe_2VAl were performed at the experimentally observed lattice constant ($a=5.75$ Å for the cubic $L2_1$ Heusler-type structure) by using the spin-polarized fully relativistic LMTO method[25,26] with the combined correction term taken into account. We used the von Barth–Hedin parametrization[27] for the exchange-correlation potential. Brillouin zone integrations were performed by using the improved tetrahedron method[28] and the charge self-consistency was obtained with 413 irreducible **k** points. The basis consisted of Fe, V, and Al s, p, and d LMTOs.

The electronic and magnetic structure of $Fe_{2-x}V_{1+x}Al$ was calculated by using a supercell approach for the compositions $x=0.031\,25$, 0.0625, 0.125, 0.25, 0.5, and 0.75. Since there are four V atoms and eight Fe atoms in the cubic $L2_1$ cell, we can construct a unit cell for $x=0.25$, as shown in Fig. 1, by replacing one of the eight Fe atoms with a V one. The positions of host atoms around a V impurity are not relaxed. Along this line, one can also prepare unit cells for smaller V concentrations starting from a $2a\times2a\times2a$ supercell of the cubic $L2_1$ lattice. Calculations for $x=0.125$ (1/8), 0.0625 (1/16), and 0.03125 (1/32) were performed by using fcc $F\bar{4}3m$ (No. 216), bcc $I\bar{4}3m$ (No. 217), and simple cubic $P\bar{4}3m$ (No. 215) unit cells, respectively, with one of Fe atoms substituted by V (V_{imp}). The latter group was also used for compositions $x=0.5$ and 0.75. It is important to note that with this choice of supercells, the distance between V impurities in the Fe sublattice is the largest possible for a given x.

The electronic structure of $Fe_{2-x}V_{1+x}Al$ for $0 \le x \le 0.125$ was also calculated by using a Koringa–Kohn–Rostoker method within the coherent potential approximation.[29] The KKR Green function method, which is formulated in terms of the multiple-scattering theory, is a well established approach for ordered and disordered systems. For these calculations, we used a full-charge density approximation in which the total energy is estimated from the nonspherical charge density and the full potential. In this approach, all radial integrals are calculated by using the unit cell geometry and only the single-site problem is solved with a spherical

potential averaged within a Voronoi cell. The accuracy of this approach is very comparable to a full-potential method and at the same time is not as time consuming. We used the cutoff angular momentum $l_{max}=3$ for the Green function expansion and the corresponding cutoff $l_{max}=6$ for the density and potential representation. The appropriate convergence with the angular momentum and normalization of the Green function was achieved by using the Lloyd formula.

The finite lifetime of a core hole was accounted for by folding the XMCD spectra with a Lorentzian. The widths of L_2 and L_3 core level spectra, with $\Gamma_{L_2}=0.78$ eV, $\Gamma_{L_3}=0.28$ eV for V and $\Gamma_{L_2}=1.14$ eV, $\Gamma_{L_3}=0.41$ eV for Fe, were taken from Ref. 30. The finite apparative resolution of the spectrometer has been accounted for by a Gaussian of 0.6 eV.

We applied the LSDA+U approach[31] as a different level of approximation to treat the electron-electron correlations. We used the rotationally invariant LSDA+U method. The implementation is described in detail in our previous paper.[32] The effective on-site Coulomb repulsion U was considered as an adjustable parameter. We used $U=4$ eV; for the exchange integral J, the value of 0.8 eV estimated from constrained LSDA calculations was used.

III. RESULTS AND DISCUSSION

A. Energy band structure

The total and partial densities of states (DOS) of Fe_2VAl, which were obtained with the LMTO method, are presented in Fig. 2. The DOS, which was obtained with the KKR method, is very similar to the LMTO findings and is therefore not shown here. The results agree well with the previous band structure calculations.[13–18] The occupied part of the valence band can be subdivided into several regions. Al 2s states appear between −9.6 and −6.05 eV. The states within the energy range of −5.8–4.0 eV are formed by Fe and V 3d states and Al 2p states. Our calculations show that Fe_2VAl is a nonmagnetic semimetal with a pronounced pseudogap at the Fermi level of around 0.2 eV width, which is in good agreement with the optical conductivity[6,7] and photoemission spectroscopy[8] measurements.

According to the T_d point symmetry of the 8c site, Fe 3d orbitals are split into a doublet e ($3z^2-1$ and x^2-y^2) and a triplet t_2 (xy, yz, and xz). V 3d states form the same double and triplet which transform according to e_g and t_{2g} irreducible representations of the O_h point group of the 4a site. The hybridization between Fe and V 3d states plays an important role in the formation of the band structure of Fe_2VAl. It leads to the splitting of the 3d states into well separated bonding and antibonding peaks. The bonding states are completely filled and have a mostly Fe e and t_2 character with the strong admixture of V t_{2g} states at about −2 eV. V e_g states give an appreciable contribution to the bonding states within the energy range of 2–4 eV below E_F. A DOS peak at −1 eV is formed by weakly antibonding Fe t_2 states.

If the Fe 3d-V 3d hybridization is turned off the band structure in the vicinity of E_F drastically changes: a peak of Fe and V 3d states appears just at the Fermi level and the semimetallic behavior is immediately lost. However, Fe 3d states of both e and t_2 symmetry still show a bonding-antibonding splitting, which confirms the importance of the Fe-Fe hybridization mentioned in Ref. 14. It is worth noting that even in the absence of the direct Fe 3d-V 3d hybridization the dispersion of V t_{2g}, and to less extent of e_g, states remains quite strong because of the V 3d-V 3d interaction mediated mainly by Fe s and p states.

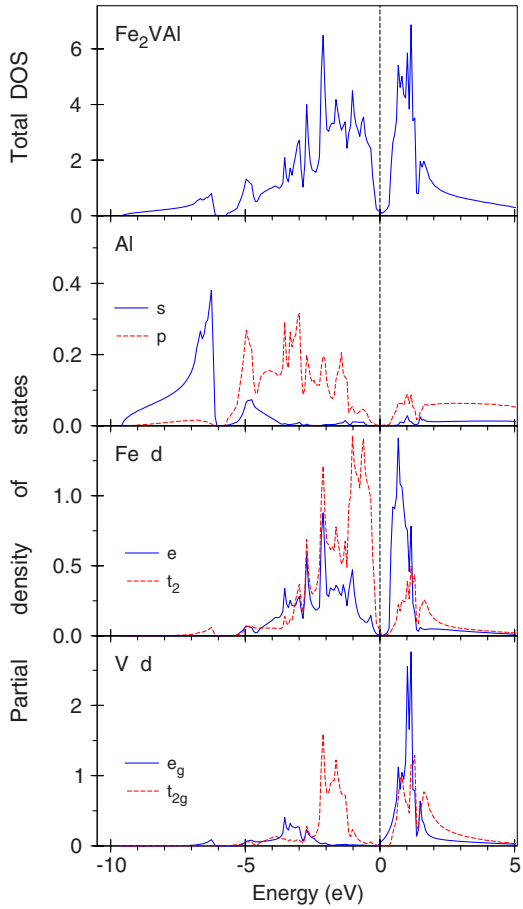

FIG. 2. (Color online) Total [in states/(cell eV)] and partial [in states/(atom eV)] densities of states of Fe_2VAl. The Fermi energy is at zero.

The Fe and V atoms in Fe_2VAl are basically nonmagnetic. However, when the $Fe_{2-x}V_{1+x}Al$ alloy has an excess of V atoms, which substitute Fe sites, they become magnetic and induce magnetic moments on neighboring sites. To describe the V impurities in Fe_2VAl, we used the CPA-KKR approach, in which impurities are embedded into a self-consistent coherent medium. The interaction between the impurities in Fe_2VAl can be approximately modeled by a differential occupation of iron positions with vanadium impurities. Within the CPA-KKR, we deal with a substitutional alloy $Fe_{1-x}V_xFe_{1-y}V_yVAl$, where x and y are the concentrations of vanadium atoms substituting, respectively, the first and the second iron atoms in the elementary unit cell of Fe_2VAl. Since the crystallographically equivalent iron sites are independently treated, this model makes it possible in a simple way to take into account short range effects. A case of $x=0$ and nonzero y models one impurity with the concentra-

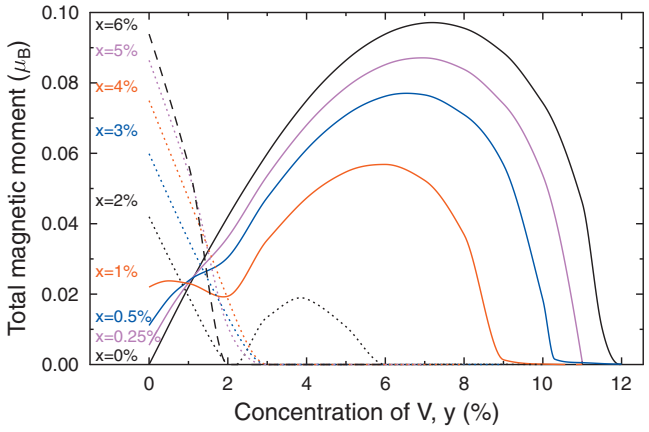

FIG. 3. (Color) Total magnetic moment per formula unit in $Fe_{1-x}V_xFe_{1-y}V_yVAl$ system for various occupations x and y of iron sites. The case $x=0$ and nonzero y corresponds to the substitution of only one iron site in the unit cell. At $x=y$, the vanadium impurities equally occupy both iron positions.

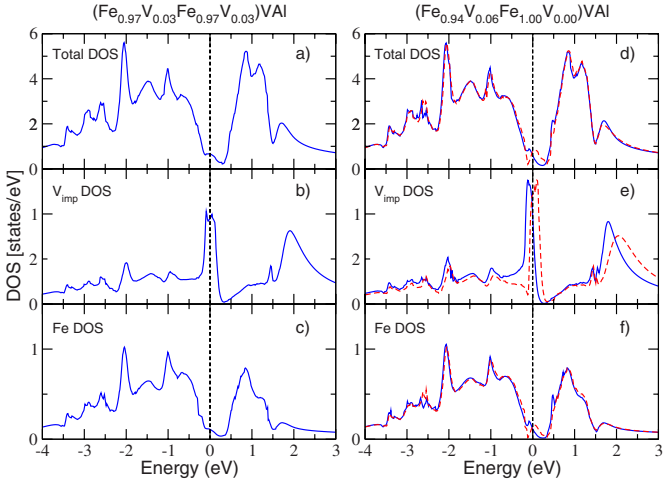

FIG. 4. (Color online) Total [in states/(cell eV)] spin-up (blue solid line) and spin-down (red dashed line) DOS, V_{imp}, and Fe resolved DOS [in states/(atom eV)] of $(Fe_{0.97}V_{0.03}Fe_{0.97}V_{0.03})VAl$ and $(Fe_{0.94}V_{0.06}Fe_{1.0}V_{0.00})VAl$. The Fermi energy is at zero.

tion y occupying only one iron position in the unit cell. The nearest neighbor impurities are substituting the same iron atom in the neighboring cells and, therefore, this corresponds to the maximal distance between impurities that can be achieved within this model. Increasing the concentration of the impurity on another iron site simulates a reduction of this distance and, hence, tunes the interaction between them. The strongest interimpurity interaction occurs in the case of $x=y$ when vanadium impurities equally substitute both iron positions.

The results of our self-consistent CPA-KKR calculations for $0 \leq (x+y) \leq 0.12$ are presented in Fig. 3. Here, the total magnetic moments of $Fe_{1-x}V_xFe_{1-y}V_yVAl$ system are shown depending on impurity concentrations x and y. By increasing the V_{imp} concentration, the total magnetic moment increases, reaching its maximum at around $y=6\%-8\%$ $(x=0)$. In this case, the total magnetic moment is contributed mainly from the impurity and iron atoms that surround the vanadium impurity and become magnetic due to the strong interaction with the impurity atom. With a further increase in the impurity concentration, the total magnetic moment rapidly decreases, vanishing at $y=0.12$ $(x=0)$. When the vanadium impurities are allowed to occupy both iron positions in the unit cell, they form much smaller local magnetic moments than in the case of $x=0$, resulting in a lower total magnetization. The nature of magnetism in $Fe_{2-x}V_{1+x}Al$ systems can be understood from the local density of states. Figures 4(a)–4(f) show the DOS calculated for the nominal composition $Fe_{1.94}V_{0.06}VAl$. In the case of $(Fe_{0.97}V_{0.03}Fe_{0.97}V_{0.03})VAl$, i.e., $x=y=0.03$, [see Figs. 4(a)–4(c)] impurities equally occupy both iron positions in the unit cell and, therefore, the V_{imp}-V_{imp} interaction is strong enough to suppress the local magnetic moments. If the same amount of vanadium occupies only one iron position in the unit cell with $x=0.06$ and $y=0$ [see Figs. 4(d)–4(f)], the distance between impurities is larger than in the previous case, and, therefore, the V_{imp}-V_{imp} hybridization is relatively weak to enable the formation of the local magnetic moment on the impurity atoms, which induce the magnetization of the nearest iron atoms [see Fig. 4(f)]. Thus, the reduction of the impurity local magnetic moment can be explained by the strong d-d hybridization between impurity atoms, which leads to the increase in the bandwidth of the impurity $3d$ band at the Fermi level and, therefore, the Stoner criterion for ferromagnetism is no longer fulfilled. The same effect occurs with the increase in the impurity concentration since it leads to a stronger interimpurity interaction as well. Thus, the magnetism in the $Fe_{1-x}V_xFe_{1-y}V_yVAl$ alloys appears due mainly to the isolated nature of impurity local moments and induced magnetic moments of their nearest iron atoms.

The CPA-KKR is a single-scattering approximation and environment effects on scattering properties are neglected except on average. This limitation does not allow to investigate the influence of atomic short-range order on the electronic properties. To simulate the atomic short-range order, we used a supercell approximation. Figure 5 shows the partial densities of states for some of nonequivalent V and Fe atoms obtained from spin-polarized calculations for $Fe_{2-x}V_{1+x}Al$ with $x=0.0625$. Here, V_1 is the V atom closest to V_{imp}, whereas Fe_1, Fe_2, and Fe_3 denote the first, second, and third Fe nearest neighbors of the V impurity, respectively. When one of Fe atoms is substituted by V, a huge narrow peak of V_{imp} $3d$ states of t_2 symmetry appears in the pseudogap of DOS exactly at E_F. In the spin-polarized calculation it is split into completely filled majority- and unoccupied minority-spin peaks, which leads to the appearance of a large spin magnetic moment of $1.2\mu_B$ at V_{imp}. The value of the moment is, however, significantly smaller than $3\mu_B$, which one would expect for a completely spin-polarized triply degenerate localized state. This indicates that the t_2 state is not completely localized on V_{imp} but extends over neighboring atoms. Indeed, an inspection of Fig. 5 shows that prominent peaks appear at the same energy in the DOS curves of Fe_1 and Fe_3 atoms. Somewhat smaller peaks can also be observed in V_1 and Fe_2 DOS, while the DOS curves of more distant V_2 and Fe_4 and Fe_5 (not shown) show only very weak features at corresponding energies. The values of

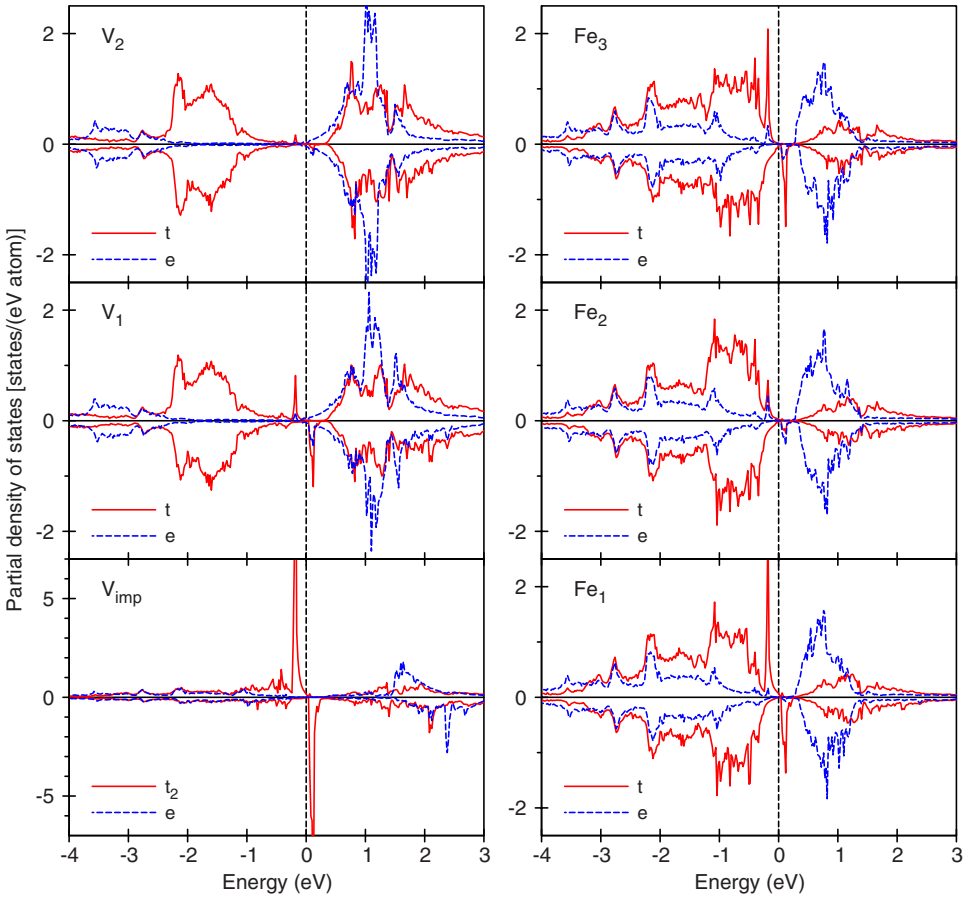

FIG. 5. (Color online) Partial [in states/(atom eV)] density of states of $Fe_{2-x}V_{1+x}Al$ ($x=0.0625$) for some of nonequivalent V and Fe atoms (see text). The DOS projected onto the xy, yz, xz (t) and $3z^2-1$ and x^2-y^2 (e) states are plotted by the solid and dashed lines, respectively. The Fermi energy is at zero.

the spin magnetic moments induced by V_{imp} on surrounding atoms correlate with the height of the DOS peaks. The largest moments of $0.16\mu_B$ and $0.15\mu_B$ are induced on Fe_1 and Fe_3 atoms. The Fe_2 moment is only $0.04\mu_B$, whereas Fe_4 ($0.003\mu_B$) and Fe_5 ($-0.01\mu_B$) moments are even smaller. Surprisingly, the moment of $0.003\mu_B$ of the nearest to the impurity V_1 atom is very small due to compensation of moments induced in V p ($0.010\mu_B$) and $3d$ ($-0.008\mu_B$) shells. The smallness and negative sign of the induced V_1 $3d$ moment indicate that it appears not due to the complete spin-polarization of the V_1 $3d$ states taking part in the formation of the V_{imp} DOS peak but rather because of hybridization of other V_1 $3d$ states with deeper lying $3d$ states of V_{imp}. The point symmetry of a V_1 site is C_{3v} with the threefold axis directed along one of four -V_{imp}-V_1-Fe_3-Al- atomic chains running along the [111] directions. With this symmetry, V_1 e_g states still transform according to a two-dimensional e representation, while the t_{2g} states are split into a singlet a_1 and a doublet e'. A more detailed analysis of symmetry-resolved V_1 $3d$ occupations shows that the contribution of the e' states, which participate in the formation of the V_{imp}-derived DOS peak, to the V_1 moment is positive. However, the contribution of the a_1 and e is larger and negative, which results in the small negative V_1 $3d$ moment.

Apparently, the narrow impurity-derived DOS peak at E_F appears as a result of the hybridization of the V_{imp} t_2 states with those Fe t_2 states that in stoichiometric Fe_2VAl do not interact with V t_{2g} states and form a peak of DOS centered at -1 eV (see Fig. 2). This explains why the contribution of the $3d$ states of the V_1 atoms, which are the closest to the impurity, to the peak at E_F is relatively small. Those of V_{imp} states that strongly hybridize with V_1 states form broad DOS features below -0.5 eV and above 1 eV, i.e., in the energy range of bonding and anti-bonding Fe t_2-V t_{2g} states, respectively (see Fig. 2).

One should mention that the V_{imp} magnetic moment obtained from the supercell calculations is not only large but robust against the change of the vanadium concentration. The spin magnetic moment of V_{imp} is equal to $1.23\mu_B$, $1.25\mu_B$, and $1.20\mu_B$ for the compositions $x\approx 0.03$, 0.06, and 0.125, respectively. Just like for $x=0.0625$, for the other two compositions, relatively large positive magnetic moments are induced on the first and third Fe neighbors around V_{imp} while the moment induced on the nearest V_1 neighbors is small and negative. In these cases, however, there are two quartets of inequivalent Fe_3 sites, $Fe_{3'}$ and $Fe_{3''}$ at the same distance from V_{imp}, situated on either -V_{imp}-V_1-$Fe_{3'}$- or -V_{imp}-Al_1-$Fe_{3''}$- chains. Calculations show that the large moment is induced only on $Fe_{3'}$ atoms that are connected to V_{imp} via V_1 atoms. It is interesting to note that in the superstructure with $x=0.125$, each $Fe_{3'}$ site is at the intersection of four V_{imp}-V_1-$Fe_{3'}$ chains. As a result, its moment of $0.51\mu_B$ is anomalously large, with the $Fe_{3''}$ moment being equal to $0.11\mu_B$. The calculation for $Fe_{2-x}V_{1+x}Al$ with $x\approx 0.03$ (1/32) gave the moments induced on Fe_1, Fe_2, and $Fe_{3'}$ ($Fe_{3''}$) as equal to $0.17\mu_B$, $0.05\mu_B$, and $0.11\mu_B$ ($0.03\mu_B$), respectively. Thus, we may conclude that at least for a small x, a region strongly polarized by magnetic V_{imp} is restricted to a tetra-

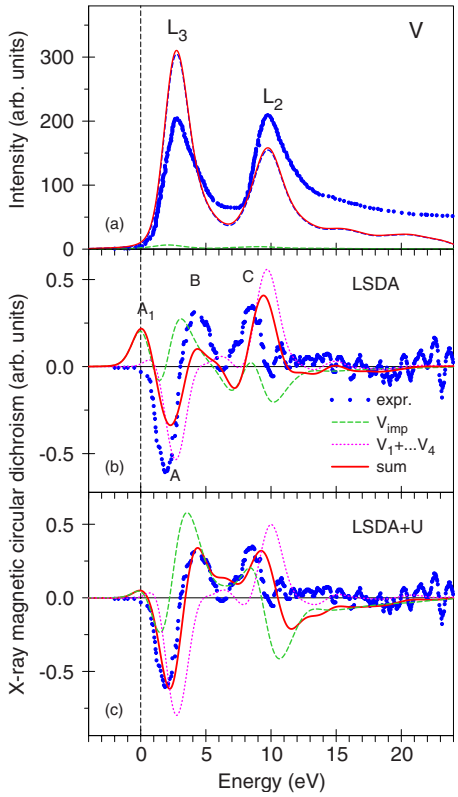

FIG. 6. (Color online) (a) Experimental isotropic absorption spectrum for the $Fe_{1.98}V_{1.02}Al$ compound (Ref. 22) (circles) at the V $L_{2,3}$ edges in comparison to the theoretically calculated spectra of $Fe_{2-x}V_{1+x}Al$ ($x \approx 0.03$) for different nonequivalent V sites [V at the Fe site, V_{imp} (dashed green line), sum of other V_1, V_2, V_3, and V_4 sites (dashed blue line), and total theoretical spectra (full red line)]; (b) experimental XMCD spectrum (Ref. 22) (circles) and the theoretically calculated XMCD spectrum in the LSDA approach at the V $L_{2,3}$ edges (full red line) with the spectra for different nonequivalent V sites: V_{imp} (dashed green line) and sum of other V sites (dotted magenta line); (c) same as (b) but for the LSDA+U calculations.

hedron formed by third Fe_3′ neighbors lying on four -V_{imp}-V_1-Fe_3′- chains. If such magnetic clusters start to overlap, one may expect a strong ferromagnetic interaction between the impurities. By increasing the V concentration, the Fermi level shifts downward in energy due to the decrease in the number of valence electrons and may reach the region of high density of the Fe 3d states. In this case, the compound becomes ferromagnetic again due to the fulfillment of the Stoner criterion on Fe atoms.

B. X-ray magnetic circular dichroism spectra

Recently, the x-ray magnetic circular dichroism in the ferromagnetic $Fe_{2-x}V_{1+x}Al$ compound (with $x=-0.07-0.08$) was studied at the transition-metal $L_{2,3}$ thresholds.[22]

Figure 6 presents the calculated XAS as well as XMCD spectra at the V $L_{2,3}$ edges for the $Fe_{2-x}V_{1+x}Al$ compound with $x \approx 0.03$ compared to the experimental data.[22] From the upper panel of Fig. 6, one can see that the theory does not reproduce the experimentally observed L_3/L_2 XAS branching ratio. It is well known that in early 3d transition metals with nearly empty 3d bands, the L_2 and L_3 absorption channels are strongly coupled through the photoelectron-core-hole Coulomb and exchange interactions.[33–36] This leads to a branching ratio of 1:1, which is far from the statistical ratio of 2:1, which is obtained in a single-particle theory, unless the spin-orbit interaction in the final 3d band is considered. From our relativistic band structure calculations, we obtained the L_3/L_2 branching ratio of 1.6.

The experimental XMCD spectrum at the V $L_{2,3}$ edges [Fig. 6(b)] is very complicated and consists of a large negative peak A at 2 eV, two positive peaks at 3.5 eV (B) and 8 eV (C), and a less intensive fine structure above 10 eV. The peaks A and B belong to the L_3 edge, while peak C and the minimum between peaks B and C are due to L_2 edge. The number of the V_{imp} atoms in the unit cell is quite small and, therefore, their contribution to the XAS is negligible in comparison to that of host V atoms [see Fig. 6(a)]. On the other hand, V_{imp} atoms play an important role in the formation of the XMCD spectrum due to their relatively large spin and orbital magnetic moments. Calculations show that the contributions of V_{imp} and host V atoms to the V $L_{2,3}$ XMCD spectrum are comparable and to a great extent compensate each other [Fig. 6(b)]. The superposition of the two contributions causes the shift of peak A to lower frequencies relative to the maximum of the L_3 XAS spectrum and the appearance of the peak B, which is completely absent in the XMCD spectrum of host V atoms. Also, because of the opposite signs of V_{imp} and host XMCD spectra, the net XMCD signal at 10 eV is rather weak. Overall, the LSDA results agree reasonably well with the experimentally measured XMCD spectrum at the V $L_{2,3}$ edges. The most prominent discrepancy is an extra peak A_1 in the LSDA spectrum that is situated just at the Fermi edge, which is not experimentally observed. The comparison of Figs. 5 and 6(b) shows that this peak is due to transitions to the minority spin t_2 states of V_{imp} that form the narrow DOS peak just above the Fermi level. Similar V XMCD spectra were also calculated for $Fe_{2-x}V_{1+x}Al$ supercell with $x \approx 0.06$. Thus, it seems that the LSDA places the narrow V_{imp}-derived DOS peak too close to the Fermi energy (Fig. 5). A possible reason for this is the underestimation of electronic correlations effects in the rather localized impurity-derived bands.

To treat the electron-electron correlations, we used the rotationally invariant LSDA+U method,[32] applying $U=4$ eV to 3d states of the V_{imp} atoms only. We found that the LSDA+U indeed improves the agreement with the experimental spectra. The narrow peak of empty 3d state is shifted upward due to the on-site Coulomb interaction U. As a result, the transitions involving the unoccupied 3d V_{imp} states occur at higher frequencies and the erroneous peak A_1 disappear from the XMCD spectra [see Fig. 6(c)]. However, two important remarks should be made: first, as discussed in Sec. III A, the t_2 states of V_{imp} are not completely localized on the impurity atom but extend over a rather large magnetic cluster. For this reason, the upward shift of the prominent peak of the V_{imp} 3d states of t_2 symmetry after application of $U=4$ eV is only 0.3 eV, i.e., significantly less than 2 eV, which one would expect for completely localized states. Second, in the present implementation of the LSDA+U method,

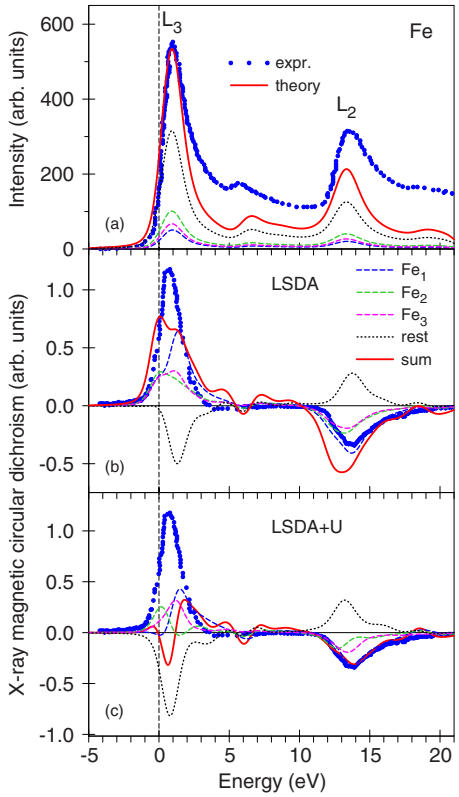

FIG. 7. (Color online) (a) Experimental isotropic absorption spectrum for $Fe_{1.98}V_{1.02}Al$ compound (Ref. 22) (circles) at the Fe $L_{2,3}$ edges in comparison to the spectra of $Fe_{2-x}V_{1+x}Al$ ($x \approx 0.03$) theoretically calculated by using the LSDA approximation for different nonequivalent Fe sites (dashed blue, green, magenta, and dotted black lines for the first, second, third Fe nearest neighbors of the V_{imp}, and sum of the rest Fe sites, respectively) and total theoretical spectrum (full red line); (b) experimental XMCD spectrum (Ref. 22) (circles) and theoretically calculated XMCD spectra in the LSDA approach at the Fe $L_{2,3}$ edges (full red line) with the spectra for different nonequivalent Fe sites; (c) same as (b) but for the LSD+U calculations.

U acts on all of the $3d$ states of V_{imp}. As a consequence, not only the localized states of t_2 symmetry taking part in the formation of the narrow DOS peaks at the vicinity of E_F but the electronic states of the whole magnetic cluster within a wide energy range are affected by U. This leads, in particular, to a strong modification of the Fe $L_{2,3}$ XMCD spectra in LSDA+U calculations. It seems that it would be more correct to apply appropriately renormalized U only to Wannier-type states responsible for the formation of the impurity-derived DOS peaks at E_F.

Figure 7 shows the XAS and XMCD spectra at the $L_{2,3}$ edges of Fe calculated in the LSDA and LSDA+U approaches together with the experimental data.[22] Among the first, second, and third Fe nearest neighbors of the V_{imp} site, the largest contribution to XAS, which is proportional to the number of Fe atoms in the corresponding shell, comes from 12 Fe_2 atoms and the smallest one from 6 Fe_1 atoms. In the XMCD spectra, the situation is quite opposite—the largest contribution comes from the Fe_1 sites due to their relatively large spin and orbital magnetic moments. More distant Fe nearest neighbors give a substantial contribution to the x-ray absorption but a relatively weak one to the XMCD spectra.

The LSDA calculations reproduce the experimental Fe $L_{2,3}$ XMCD spectra reasonably well, although the calculated magnetic dichroism is somewhat too low at the L_2 edge and too high at the L_2 one. The LSDA+U improves the agreement with the experiment for the L_2 edge but gives an unsatisfactory description of the dichroism at the L_3 edge, which is probably due to the reasons we discussed above.

IV. SUMMARY

The Fe and V atoms in Fe_2VAl are basically nonmagnetic. However, when the $Fe_{2-x}V_{1+x}Al$ alloy has an excess of V atoms (V_{imp}), they enter into the Fe sites, and acquire a magnetic moment of approximately $1.2\mu_B$/V. Moreover, Fe atoms in the original Fe sublattice also possess magnetic moments. V_{imp} atoms give rise to magnetic clusters. A cluster contains a tetrahedron from the first V neighbors, an octahedron from the first Fe neighbors, and another tetrahedron larger in size from the third Fe neighbors. The magnetic disturbance generated by V_{imp} locates in this volume.

By increasing the concentration x, the direct V_{imp}-V_{imp} hybridization gets stronger and the width of the prominent peaks at close vicinity of the Fermi level increases. As the consequence, V_{imp} atoms loses the magnetic moment and the compound becomes nonmagnetic. If we continue to increase the V concentration, the Fermi level is shifted downward in energy due to a decrease in the valence electron concentration and may reach high Fe $3d$ DOS. In this case the compound, becomes ferromagnetic again due to fulfillment of Stoner criteria on Fe atoms.

We have studied the electronic structure and x-ray magnetic circular dichroism spectra in the ferromagnetic phases of $Fe_{2-x}V_{1+x}Al$ compound within the LSDA as well as LSDA+U approximations by means of an *ab initio* fully relativistic spin-polarized Dirac linear muffin-tin orbital method. We found that the contribution from the V_{imp} atoms to the x-ray absorption spectra are insignificant. On the other hand, V_{imp} atoms play major role in the XMCD spectra due to their relatively large spin and orbital magnetic moments. The calculated XMCD spectra at the V $L_{2,3}$ edge in the LSDA approach show good agreement with the experiment except for an additional peak at the Fermi edge, which is not experimentally observed. The LSDA+U approximation moves this peak toward a higher energy, improving the agreement with the experimental spectra.

*aernst@mpi-halle.de

[1] Y. Nishino, M. Kato, S. Asano, K. Soda, M. Hayasaki, and U. Mizutani, Phys. Rev. Lett. **79**, 1909 (1997).
[2] M. Kato, Y. Nishino, U. Mizutani, and S. Asano, J. Phys.: Condens. Matter **12**, 1769 (2000).
[3] C. S. Lue and J. J. H. Ross, Phys. Rev. B **58**, 9763 (1998).
[4] C. S. Lue and J. J. H. Ross, Phys. Rev. B **61**, 9863 (2000).
[5] M. Kato, Y. Nishino, S. Asano, and S. Ohara, J. Jpn. Inst. Met. **62**, 669 (1998).
[6] H. Okamura *et al.*, Phys. Rev. Lett. **84**, 3674 (2000).
[7] Y. Feng, J. Y. Rhee, T. A. Wiener, D. W. Lynch, B. E. Hubbard, A. J. Sievers, D. L. Schlagel, T. A. Lograsso, and L. L. Miller, Phys. Rev. B **63**, 165109 (2001).
[8] K. Soda *et al.*, J. Synchrotron Radiat. **9**, 233 (2002).
[9] N. Kawamiya, Y. Nishino, M. Matsuo, and S. Asano, Phys. Rev. B **44**, 12406 (1991).
[10] K. Endo, H. Matsuda, K. Ooiwa, M. Iijima, K. Ito, T. Goto, and A. Ono, J. Phys. Soc. Jpn. **66**, 1257 (1997).
[11] S. Fujii, Y. Ienaga, S. Ishida, and S. Asano, J. Phys. Soc. Jpn. **72**, 698 (2003).
[12] Y. Nishino, H. Sumi, and U. Mizutani, Phys. Rev. B **71**, 094425 (2005).
[13] G. Y. Guo, G. A. Botton, and Y. Nishino, J. Phys.: Condens. Matter **10**, L119 (1998).
[14] D. J. Singh and I. I. Mazin, Phys. Rev. B **57**, 14352 (1998).
[15] R. Weht and W. E. Pickett, Phys. Rev. B **58**, 6855 (1998).
[16] M. Weinert and R. E. Watson, Phys. Rev. B **58**, 9732 (1998).
[17] A. Bansil, S. Kaprzyk, P. E. Mijnarends, and J. Tobola, Phys. Rev. B **60**, 13396 (1999).
[18] G. A. Botton, Y. Nishino, and C. J. Humphreys, Intermetallics **8**, 1209 (2000).
[19] J. Deniszczyk, Acta Phys. Pol. B **32**, 529 (2001).
[20] H. Sumi, M. Kato, Y. Nishino, S. Asano, and U. Mizutani, J. Jpn. Inst. Met. **65**, 771 (2001).
[21] O. Yoshimoto *et al.*, J. Synchrotron Radiat. **8**, 457 (2001).
[22] K. Soda *et al.*, Physica B (Amsterdam) **351**, 338 (2004).
[23] V. Antonov, B. Harmon, and A. Yaresko, *Electronic Structure and Magneto-Optical Properties of Solids* (Kluwer, Dordrecht, 2004).
[24] V. N. Antonov, B. N. Harmon, A. N. Yaresko, and A. P. Shpak, Phys. Rev. B **75**, 165114 (2007).
[25] O. K. Andersen, Phys. Rev. B **12**, 3060 (1975).
[26] V. V. Nemoshkalenko and V. N. Antonov, *Computational Methods in Solid State Physics* (Gordon and Breach, Amsterdam, 1998).
[27] U. von Barth and L. Hedin, J. Phys. C **5**, 1629 (1972).
[28] P. E. Blöchl, O. Jepsen, and O. K. Andersen, Phys. Rev. B **49**, 16223 (1994).
[29] G. M. Stocks, W. M. Temmerman, and B. L. Gyorffy, Phys. Rev. Lett. **41**, 339 (1978).
[30] J. L. Campbell and T. Parr, At. Data Nucl. Data Tables **77**, 1 (2001).
[31] V. I. Anisimov, J. Zaanen, and O. K. Andersen, Phys. Rev. B **44**, 943 (1991).
[32] A. N. Yaresko, V. N. Antonov, and P. Fulde, Phys. Rev. B **67**, 155103 (2003).
[33] J. Zaanen, G. A. Sawatzky, J. Fink, W. Speier, and J. C. Fuggle, Phys. Rev. B **32**, 4905 (1985).
[34] J. Schwitalla and H. Ebert, Phys. Rev. Lett. **80**, 4586 (1998).
[35] P. Krüger and C. R. Natoli, Phys. Rev. B **70**, 245120 (2004).
[36] A. L. Ankudinov, A. I. Nesvizhskii, and J. J. Rehr, Phys. Rev. B **67**, 115120 (2003).